



HAL
open science

Flexure of the Lithosphere Beneath the North Polar Cap of Mars: Implications for Ice Composition and Heat Flow

A. Broquet, M. Wiczorek, W. Fa

► **To cite this version:**

A. Broquet, M. Wiczorek, W. Fa. Flexure of the Lithosphere Beneath the North Polar Cap of Mars: Implications for Ice Composition and Heat Flow. *Geophysical Research Letters*, 2020, 47 (5), 10.1029/2019GL086746 . hal-02980448

HAL Id: hal-02980448

<https://hal.science/hal-02980448>

Submitted on 15 Apr 2022

HAL is a multi-disciplinary open access archive for the deposit and dissemination of scientific research documents, whether they are published or not. The documents may come from teaching and research institutions in France or abroad, or from public or private research centers.

L'archive ouverte pluridisciplinaire **HAL**, est destinée au dépôt et à la diffusion de documents scientifiques de niveau recherche, publiés ou non, émanant des établissements d'enseignement et de recherche français ou étrangers, des laboratoires publics ou privés.

Copyright

Geophysical Research Letters

RESEARCH LETTER

10.1029/2019GL086746

Special Section:

InSight at Mars

Key Points:

- Radar data and a flexural loading model are used to probe the composition of the north polar cap of Mars and the strength of the lithosphere
- The elastic thickness beneath the north polar cap is found to be between 330 and 450 km, implying regional heat flows of 11 to 16 mW m⁻²
- For reasonable dust contents, large quantities of CO₂ ice must be mixed within the polar cap to be consistent with our inferred compositions

Supporting Information:

- Supporting Information S1

Correspondence to:

A. Broquet,
 adrien.broquet@oca.eu

Citation:

Broquet, A., Wiczeorek, M. A., & Fa, W. (2020). Flexure of the lithosphere beneath the north polar cap of Mars: Implications for ice composition and heat flow. *Geophysical Research Letters*, 47, e2019GL086746. <https://doi.org/10.1029/2019GL086746>

Received 20 DEC 2019

Accepted 25 FEB 2020

Accepted article online 26 FEB 2020

Flexure of the Lithosphere Beneath the North Polar Cap of Mars: Implications for Ice Composition and Heat Flow

A. Broquet¹ , M. A. Wiczeorek¹ , and W. Fa^{2,3} 

¹Observatoire de la Côte d'Azur, CNRS, Laboratoire Lagrange, Université Côte d'Azur, Nice, France, ²Institute of Remote Sensing and Geographical Information System, School of Earth and Space Sciences, Peking University, Beijing, China, ³State Key Laboratory of Lunar and Planetary Sciences, Macau University of Science and Technology, Macau, China

Abstract The geodynamical response of the lithosphere under stresses imposed by the geologically young north polar cap is one of the few clues we have to constrain both the polar cap composition and the present-day thermal state of Mars. Here we combine radar data with a flexural loading model to self-consistently estimate the density (ρ) and real dielectric constant (ϵ') of the polar cap, and the elastic thickness of the lithosphere underneath (T_e). Our results show that ρ ranges from 920 to 1,520 kg m⁻³, ϵ' is 2.75 (+0.40, -0.35), and T_e is between 330 and 450 km. We determine a polar cap volume that is up to 30% larger than current estimates that all neglect lithospheric flexure. Our inferred compositions suggest that, for dust content larger than about 6 vol%, 10 vol% CO₂ ice is mixed within the polar deposits, which has important implications for the climate evolution of Mars.

Plain Language Summary The north polar cap of Mars is a tremendous reservoir of ices and dust of unknown concentration and composition. It is transparent to radar giving us a unique insight into its structure and composition. Here we use a novel technique that combines radar and elevation data along with a flexure model, to invert for the polar cap composition and the strength of the underlying lithosphere. Similar to previous studies, we find that the lithosphere below the north pole is extremely rigid and does not deform much under the load of the polar cap. This implies that the north polar region is currently colder than the rest of the planet, which has profound implications for our understanding of the structure and evolution of the Martian interior. Our inferred compositions suggest that for reasonable dust contents, about 10 vol% CO₂ ice is mixed within the polar deposits. This is the first time a large quantity of CO₂ ice is constrained to exist in the north polar cap. Like on Earth, where the composition of buried ices gives hints on the climatic evolution, having CO₂ ice at the north pole of Mars will help improve scenarios for the climate evolution of the planet.

1. Introduction

The Martian north polar cap has long been recognized to be a tremendous reservoir of water ice and possibly dry ice or even clathrate-hydrates (Mellon, 1996). The geologically young (<4 Ma, see Herkenhoff & Plaut, 2000; Levrard et al., 2007) polar cap plays a significant role in the present-day Martian climate, and its stratigraphically layered deposits are a witness to the planet's climate evolution (Nerozzi & Holt, 2019). The cap acts as a large-scale load that can bend the underlying and surrounding basement. Analysis of the associated lithospheric flexure is one of the few methods that give access to the composition of the polar cap and to the present-day strength of the lithosphere, which is related to the thermal state of the planet (e.g., Phillips et al., 2008; Plesa et al., 2018).

Radar sounding data from MARSIS (Mars Advanced Radar for Subsurface and Ionosphere Sounding) on Mars Express and SHARAD (SHALLOW RADAR) onboard Mars Reconnaissance Orbiter have been extensively used to unveil the structure of the north polar deposits (Byrne, 2009). The two instruments operate at frequencies of 1.3–5.5 MHz and 20 MHz, allowing them to probe depths from several hundreds of meters to several kilometers with range resolutions in vacuum of 150 m for MARSIS (Picardi et al., 2005) and 15 m for SHARAD (Phillips et al., 2008). The bulk of the north polar cap is made of the north polar layered deposits that are thought to consist of nearly pure water ice (Grima et al., 2009; Selvens et al., 2010). These deposits overlay a basal unit with a more limited extent and whose composition is believed to have a larger quantity

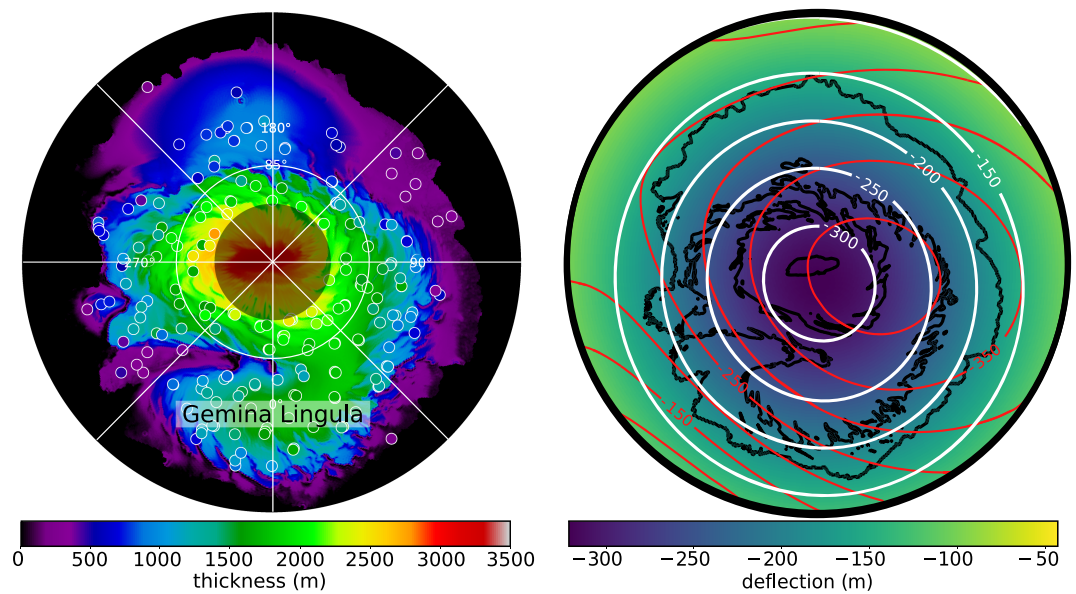


Figure 1. (left) Estimated thickness of the north polar cap from MOLA surface elevations under the assumption that the base of the cap follows the regional slope. The filled colored circles correspond to the thickness obtained at 213 regions from MARSIS radargrams. (right) Computed lithospheric deflection from our model (color map and white contours) and that of Phillips et al. (2008) (red contours), for $T_e = 300$ km and $\rho = 1,100$ kg m⁻³. For context, elevation contours of the polar cap are plotted as black lines.

of dust (Herkenhoff et al., 2007; Nerozzi & Holt, 2019). Both MARSIS and SHARAD observed a general lack of downward deflection below the north polar cap with uncertainties of about 200 m everywhere (Selvans et al., 2010) and 100 m across Gemina Lingula (Phillips et al., 2008) (Figure 1).

The absence of measurable lithospheric flexure in these previous studies suggests that the thickness of the elastic lithosphere is more than 300 km and that Mars might be colder than once thought (Phillips et al., 2008). The joint spectral analysis of gravity and topography also constrained the present-day elastic thickness for the south pole to be high, at least 108 km (Wieczorek, 2008). These high (and potentially different) elastic thickness values at the north and south poles are difficult to reconcile with current thermal evolution models (e.g., Plesa et al., 2018).

These inferences, however, could be flawed given that there are significant uncertainties that could hide the signal of lithospheric deflection. The global uncertainty on the basal deflection given by analyses of MARSIS data in Selvans et al. (2010) was for a single value of the real part of the complex dielectric constant (ϵ' , hereafter abbreviated to dielectric constant), where it was assumed that the whole polar cap was made of nearly pure water ice with $\epsilon' = 3$. As the polar cap thickness scales as $1/\sqrt{\epsilon'}$, varying ϵ' can significantly increase this uncertainty. The study of Phillips et al. (2008) used the global topography as a load when predicting the deflection of the lithosphere, and the presence of a long-wavelength signal arising from the broad Tharsis volcanic province could bias the lithospheric deflection beneath the polar cap. Lastly, we note that constraints on the composition of the polar cap were obtained by assuming that its base is flat and inverting for the dielectric constant using Mars Orbiter Laser Altimeter (MOLA) elevation and radar data (e.g., Grima et al., 2009; Nerozzi & Holt, 2019). If the base were deflected downward, this would require a lower bulk dielectric constant of the polar cap and modify the inferred compositions.

In this study, we combine MARSIS and SHARAD radar data and MOLA elevation data with an improved elastic loading model to jointly invert for the density and dielectric constant of the polar cap and the elastic thickness of the lithosphere underneath. We refine and give a more robust elastic thickness estimate that will help to constrain interior models using data from the InSight mission (Plesa et al., 2018; Smrekar et al., 2018). We further give a new estimate of the north polar cap volume, which is up to 30% higher than previous studies that neglected lithospheric flexure. We finally constrain that, when considering reasonable dust contents, there must be large quantities of CO₂ ice mixed within the north polar perennial cap, which has important implications for the climate evolution of Mars.

2. Inversion for Elastic Thickness, Density, and Dielectric Constant

We invert for the elastic thickness of the lithosphere (T_e), the polar cap load density (ρ), and the dielectric constant by minimizing the root-mean-square (rms) misfit of the function

$$\psi(\epsilon', T_e, \rho) = [h_e - h_0 - W(T_e, \rho)] - h_t(\epsilon'). \quad (1)$$

In this equation, h_e is surface elevation, h_0 is an estimated preloading surface topography, W is the computed deflection of the polar cap basement, and h_t is the thickness of the polar cap derived from radar data. All terms depend implicitly on position. The first term in square brackets represents the thickness of the polar cap at a given location based on the surface elevation and lithospheric deflection and is dependent on the density of the polar cap and the elastic thickness. The last term is a measurement of the thickness from radar data, which depends on the assumed dielectric constant.

For our calculations, it is necessary to have an estimate of the shape of the surface before the polar cap formed. The preloading surface elevation (h_0) was estimated using an annulus of MOLA elevation data (Smith et al., 2001) exterior to the polar cap between 70°N and 75°N (see also Selvans et al., 2010), and these data were interpolated poleward using the minimum curvature method of Smith and Wessel (1990). The preloading surface follows the long-wavelength regional topography that slopes from high values north of Arabia Terra near 90° E toward Alba Mons near 270° E (supporting information Figure S1). We note that varying the annulus latitudinal limits by $\pm 2^\circ$ introduces an rms difference of only 170 m in the elevation of the basement.

The radar thickness (h_t) was derived from MARSIS and SHARAD data. We picked manually 213 locations that are spatially scattered across the polar deposits, investigated all available radargrams, and identified visually the reflections arising from the icy surface and the ice/substratum interface. The surface reflectors were selected as those echoes with the strongest amplitude and with the shortest time delay, and the deepest subsurface reflectors were identified as the strongest echoes with the largest time delay (Figure S2). For each location, the lateral continuity of the surface and subsurface reflectors were verified to extend at least seven frames along the orbital track (corresponding to a horizontal distance of about 35 km). The thickness is calculated using the time delay between the surface and subsurface echoes (t) and then converting the result into a distance by assuming a value for ϵ'

$$h_t = \frac{ct}{2\sqrt{\epsilon'}}, \quad (2)$$

where c is the speed of light in vacuum.

The elastic deflection (W) is computed using the load model of Belleguic et al. (2005) (see also Broquet & Wiczorek, 2019) that improves upon the model used in Phillips et al. (2008) by better accounting for the restoring normal stresses and self-gravitational effects. Since the load depends explicitly upon (W) and the density (ρ), we first define the load thickness from MOLA surface elevations and the initial preloading surface ($h_e - h_0$) and then iterate by adding the amount of corresponding deflected materials. Typically, only a few iterations are necessary to converge to submeter accuracies. As in Phillips et al. (2008), the densities of the crust and mantle were set to 2,900 and 3,500 kg m⁻³, respectively, the crustal thickness (T_c) was set to 35 km, Young's modulus (E) was set to 100 GPa, and Poisson's ratio (ν) was assumed to be 0.25. Variation of 200 kg m⁻³ for the crust or mantle densities and 30% variation in E , ν , or T_c only result in less than 10% variation in T_e .

3. Polar Cap Thickness and Lithospheric Deflection

In Figure 1 (left), we plot an estimated thickness of the north polar cap from MOLA surface elevations under the assumption that the base of the cap follows the regional slope. In this image, the polar cap has a maximum thickness of 3,120 m and a volume of 1.31×10^6 km³, which are consistent with earlier studies (e.g., Selvans et al., 2010). Superposed on this map, we plot the polar cap thickness as determined by our 213 MARSIS measurements, with the fill color corresponding to the same color scale as the main image, where we have assumed that $\epsilon' = 3$ (e.g., Selvans et al., 2010). Given that the spacecraft orbit is not perfectly polar, there are no observations poleward 87°N. A good overall agreement between the estimated thickness and radar measurements is seen. Small differences are likely due to local variations in dielectric constant and/or

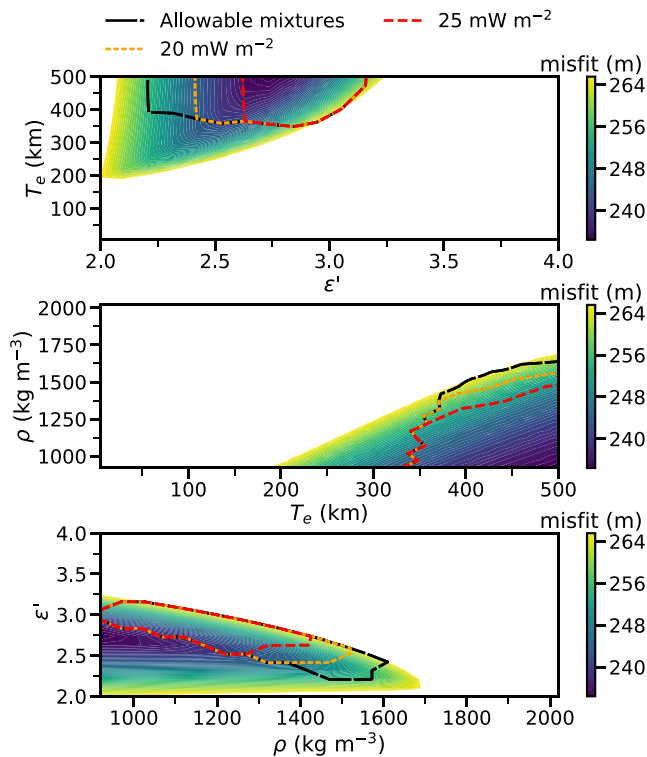


Figure 2. Minimum rms misfit as a function of the dielectric constant (ϵ'), elastic thickness (T_e), and bulk density of the polar cap (ρ) using MARSIS data at 213 locations. The color corresponds to the rms misfit that is cut off at 266 m. The black lines delimit possible mixtures, and the red and orange lines delimit those same mixtures that do not produce basal melting for heat flows of 20 and 25 mW m⁻².

to lithospheric deflection beneath the polar deposits. We also investigated SHARAD data and observed that the thickness predictions are in good agreement with MARSIS where the basal unit is not present. SHARAD cannot generally see through the entirety of the basal unit as a result of its shallow penetration depth in sand-rich deposits (see Text S1 and Figure S2 and Nunes & Phillips, 2006).

On the right panel of Figure 1, we reproduce the deflection of the lithosphere from Phillips et al. (2008) in red, for an elastic thickness of 300 km and a surface density of 1,100 kg m⁻³. The deflection using our model for the same parameters is shown in white and is due solely to the isolated load of the polar cap. Though both contours fit the condition of less than 100 m of relative deflection across Gemina Lingula, there are significant differences. The deflection of Phillips et al. (2008) is offset from the center of the polar cap, with about 400 m of deflection near the center and more than 350 m of deflection outside of the polar cap. In comparison, the deflection computed from our model that is centered on the polar cap has a slightly smaller central value of 320 m and has less than 150 m of deflection outside of the polar cap.

We found that this difference was due to Phillips et al. (2008) using the global topography as a load (with a constant density of 1,100 kg m⁻³) in the deflection model, causing the presence of an unwanted long-wavelength signal originating from the broad Tharsis province. It is clear that Tharsis formed billions of years before the polar cap was emplaced and that its induced flexure is unrelated to the flexure resulting from the geologically young polar cap. Given that our polar cap load is defined with respect to the regional topographic slope, any ancient flexural signature resulting from Tharsis is already represented in the regional topography that is being interpolated beneath the polar cap.

4. Results

We show in Figure 2 the minimum misfit of equation (1) as a function of two parameters and for any value of the third parameter. The misfit was computed using MARSIS data at 213 locations, of which the number is more than sufficient to obtain robust estimates and uncertainties of the three free parameters in our inversion (see Figure S3). The rms misfit is cut off at 266 m, which is the maximum allowed misfit in the estimation of the thickness of the polar cap that includes the range resolution of MARSIS, surface roughness at the scale of the Fresnel zone of MARSIS, and the uncertainty in the estimation of the preloading surface (see Text S2 for more details).

We observe that the dielectric constant ranges from 2.00 (the minimum value investigated) to 3.25 with a best fit of about 2.75, the elastic thickness must be greater than 180 km, and the density must be less than 1,700 kg m⁻³. The minimum required elastic thickness is significantly lower than the 300 km obtained by Phillips et al. (2008) as a result of the improved loading model. We will see that including additional constraints that were not considered by Phillips et al. (2008) will require an increase in the minimum elastic thickness. We note that when assuming zero deflection (i.e., an infinite elastic thickness), the obtained dielectric constant is 3.14 ± 0.35 , which is similar to that found in Grima et al. (2009) who assumed zero deflection.

Parts of the colored regions of Figure 2 correspond to densities and dielectric constants that cannot be simultaneously obtained by mixtures of ices and dust. A three-component Maxwell-Garnett mixing law (Sihvola, 2000) was used to compute the bulk dielectric constant where we assumed that the matrix was the component with the largest volumetric abundance. We note that the results would be similar using a power law mixing relation as in Nerozzi and Holt (2019). The dielectric constants for solid CO₂, H₂O ice, and dust were set to 2.2, 3, and 6, respectively, and the densities of solid CO₂ and water ice were assumed to be 1,560 and 920 kg m⁻³. The density of the dust component was allowed to vary from 2,200 to 3,400 kg m⁻³, which covers the range from gypsum to basalt (Nunes & Phillips, 2006). The range of solutions that fit the data and

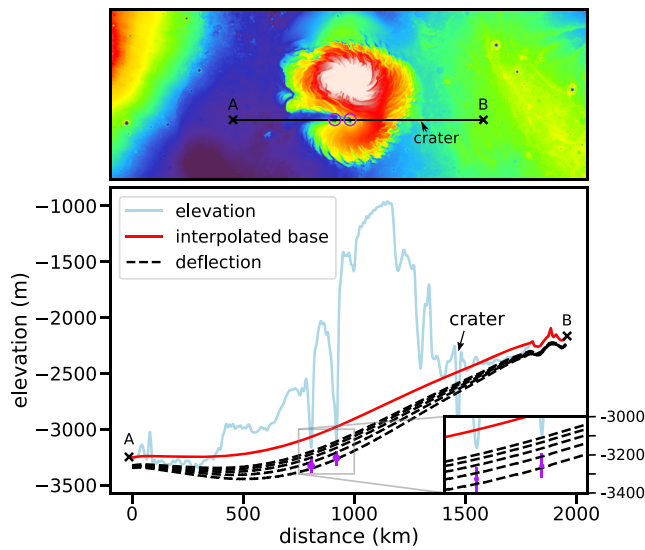


Figure 3. Surface and deflection profiles across Chasma Boreale. The profile section and deepest troughs are shown in the upper image. In the lower image, we display an elevation profile based on MOLA data (blue), a profile for the interpolated basement (red), and several profiles of lithospheric deflection (dashed black). The deflection profiles were computed for $T_e = 300$ (lower) to 500 (upper) km with 50 km increments and $\rho = 1,100 \text{ kg m}^{-3}$. The inset shows details regarding two SHARAD measurements of the base of the polar cap (purple), where we set $\epsilon' = 3.5$. The interpolated basement is seen to extend above the MOLA profile by a few tens of meters, from a distance of 90 to 360 km and from 1,550 to 1,750 km. This is due to local topographic variations with wavelengths that are smaller than those used in defining the interpolated basement.

that can also be accounted for by a mixture of these three components is outlined by the black dashed line in this figure. The range of permissible values for the dielectric constant is reduced to 2.2 to 3.15, the minimum elastic thickness is increased to 330 km, and the maximum density is reduced to $1,600 \text{ kg m}^{-3}$.

We further note that the thermal conductivity of the polar cap is strongly dependent on the relative abundances of ices and dust (Mellon, 1996; Wieczorek, 2008). If the effective thermal conductivity is low enough, this could result in temperatures that would be sufficient to melt the base of the cap (see Text S3 for more details). In regions covered by radar observations, there is no evidence for a melt layer being present today, and we thus assume that basal melting is not presently occurring. The orange and red dashed lines delimit the allowable compositions that do not generate basal melting under typical heat flows of 20 and 25 mW m^{-2} (Plesa et al., 2018). For a heat flow of 20 mW m^{-2} , the dielectric constant is found to range from 2.40 to 3.15, the elastic thickness is found to be independent of heat flow with a value of at least 330 km, and the density is found to range from 920 to $1,520 \text{ kg m}^{-3}$. The obtained range of densities is in good agreement with gravity studies at the north (Ojha, Nerozzi, & Lewis, 2019) and south (Wieczorek, 2008; Zuber et al., 2007) poles where the bulk density of both caps was found to be about $1,200 \pm 150 \text{ kg m}^{-3}$.

We performed an independent inversion using SHARAD data, but only at 78 restricted locations where the basal unit is not present and where the base of the polar cap is clearly visible (Figure S2). The results we obtained were generally consistent with those presented above, but with a slightly higher elastic thickness and lower dielectric constant (Figure S4). As an example, for a heat flow of 20 mW m^{-2} , the dielectric constant was found to range from 2.4 to 3.0, the elastic thickness was found to be at least 370 km, and the surface density was constrained to be less than $1,570 \text{ kg m}^{-3}$.

We note that the only way to lower the elastic thickness at the north pole would be to simultaneously reduce the density and dielectric constant of the mixture. This could be achieved by adding some porosity, and for 2 or 5 vol% porosity, the minimum elastic thickness would be reduced to respectively 300 and 280 km. On Earth, a typical volume fraction of bubbles in glacial ice at an equivalent Martian depth of 1,200 m is only about 0.5% (Fegyveresi et al., 2016), so the presence of porosity would likely have only a small effect on our inversion results.

In Figure 3, we show a map of the polar cap and several profiles across Chasma Boreale. Chasma Boreale is a deep trough that separates the main lobe of the north polar cap from Gemina Lingula (Figure 3). Radar studies have shown that the basal unit is exposed at the bottom of Chasma Boreale where it is only about 150 m thick (Holt et al., 2010; Putzig et al., 2009; Selvans et al., 2010). Using SHARAD data, we confirmed that the thickness of the basal unit in the two deepest troughs of Chasma Boreale is about 150 m. These two troughs are located close to the center of the polar cap, where the basement is potentially subject to a large deflection, which makes them remarkably sensitive to variations in elastic thickness such that we decided to treat them separately.

The bottom panel of Figure 3 plots several profiles including the surface elevation as defined by MOLA (blue), the preloading surface (red), and deflection profiles for various elastic thicknesses (black). The two purple dots correspond to the base of the basal unit given by SHARAD in the two deepest troughs of Chasma Boreale that is 150 m below the local surface elevation given by MOLA. We have considered a 65 m depth uncertainty at these locations that corresponds to plausible variations in the dielectric constant (from 2.5 to 3.5), uncertainties from the preloading surface and surface roughness, and the range resolution of SHARAD. At these locations, we observe that the preloading surface is about 230 m above the basement depth given by SHARAD. A small amount of deflection of the surface is thus required to account for these measurements. Based on the plotted deflection profiles, we observe that the elastic thickness has a best fit of about

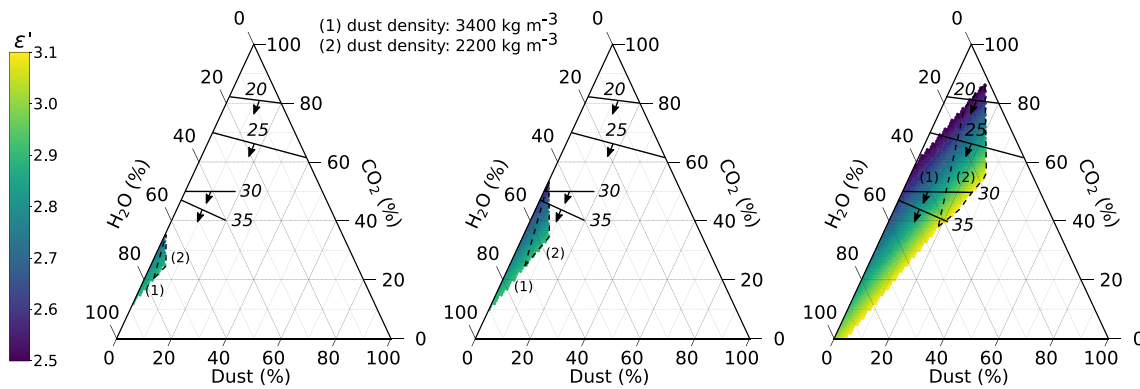


Figure 4. Ternary plot for allowable volumetric mixtures of ices and dust for three elastic thicknesses, 330, 350, and 400 km (from left to right), where the color corresponds to the dielectric constant. The black lines limit the regions beyond which basal melting will occur as a function of various heat flows from 20 to 35 mW m^{-2} with acceptable solutions in the direction given by the black arrows. The dashed lines show the accepted mixtures that must be added if the dust density is decreased from (1) 3,400 to (2) 2,200 kg m^{-3} .

320 km and cannot be larger than 400 km. We note that if the load density is set to the highest allowed value (1,520 kg m^{-3}), then the largest allowable elastic thickness is 450 km.

5. Composition of the North Polar Cap

To address the composition of the north polar cap, we assumed that the polar cap is homogeneous and explored which fractions of H_2O and CO_2 ices and dust (clathrates are treated in Text S4 and Figure S5) could fit both our density and dielectric constant estimates. Given that both parameters are dependent on the elastic thickness, we show three results in Figure 4 for three different elastic thicknesses (330, 350, and 400 km). Each plot is a ternary diagram that shows the range of allowable compositions, where the color represents the corresponding dielectric constant of the mixture. In all cases, we observe that the north pole is made mostly of pure water ice and that high heat flows require a low solid CO_2 content in order to not melt the base of the cap.

For an elastic thickness of 330 or 350 km, we observe that there must be at least 10 vol% dry ice within the north polar deposits and that the dielectric constant of the allowed compositions ranges from 2.7 to 2.9. Only the larger elastic thickness of 400 km allows for a solid CO_2 free polar cap when the dust content is less than 5 vol%. However, having less than 5 vol% of dust within the north polar cap is inconsistent with the results of Nerozzi and Holt (2019). These authors constrained the minimum dust content of the basal unit to be about 18%, which translates to an average of 6 vol% dust for the entire north polar cap, assuming that the basal unit is 35% the volume of the cap (Selvans et al., 2010). We thus dismiss cases with dust contents less than 5 vol%, and when it is larger than 6 and 8 vol%, the polar cap is required to have at least 8 and 13 vol% dry ice, respectively. The maximum volume fraction of dust in the polar cap is found to depend upon the elastic thickness and dust density and varies from 5% to 28%. If the polar cap does not contain CO_2 , but instead clathrate ices, there must be at least 77 vol% clathrate ices for a heat flow of 20 mW m^{-2} , which is unlikely (Figure S5).

6. Discussion

Using the formalism of McNutt (1984) and accounting for heat-producing elements (HPEs) in the crust (Hahn et al., 2011), the minimum 330 and maximum 450 km elastic thicknesses can be shown to imply surface heat flows of 16 and 11 mW m^{-2} (see Text S4). In a recent study, Ojha, Karimi, et al. (2019) computed lithospheric deflection profiles beneath the north polar cap as a function of heat flow using a more sophisticated finite element method with a visco-elastoplastic rheology. Our results imply a maximum absolute deflection of 400 m at the center of the polar cap and 250 m below Gemina Lingula. From Figure 2 of Ojha, Karimi, et al. (2019), our constraints require the mantle heat flow to be 13 to 20 mW m^{-2} .

Using previously reported MARSIS and SHARAD radar constraints on the amount of lithospheric deflection beneath the north polar cap, Ojha, Karimi, et al. (2019), however, inferred a considerably lower mantle heat flow of 7 mW m^{-2} . This discrepancy is largely the result of their having mistook previously reported relative

deflections between two points with the maximum absolute deflection below the deposit (see Figure S7). For example, the maximum deflection at the center of the cap, as predicted by both Phillips et al. (2008) and this study, is about 350–400 m. Ojha, Karimi, et al. (2019) however used a value of 200 m, but this value (Selvans et al., 2010) represents only the relative deflection from the edge of the cap to about half-way to the center of the polar cap.

In a suite of thermal evolution models, Plesa et al. (2018) investigated how the thickness of the crust (which is enriched in HPE) affects the thickness of the lithosphere. For these models, that have a chondritic abundance of HPE, an elastic thickness of more than 330 km at the north pole was compatible with an average crustal thickness of about 60 to 87 km. Nevertheless, if the concentration of HPE in the crust is twice the reference value given by gamma ray spectroscopy measurements (e.g., Hahn et al., 2011), one model with a lower crustal thickness (29.5 km) can satisfy our constraints on T_e (see also Thiriet et al., 2018).

There are a few complications to our model that could perhaps provide a lower elastic thickness at the north pole. It is possible that the polar cap load is not yet at elastic equilibrium but is rather in a transient state, undergoing downward deflection, as a result of viscous relaxation. The north polar region could also be experiencing some level of postglacial rebound (upward deflection) from a former larger cap that is competing with the present-day deflection. The presently observed deflection would then be the sum of these two components, which would lead to an overestimation of the elastic thickness. Although elastic equilibrium can be achieved on a timescale shorter than the age of the north polar cap (e.g., Phillips et al., 2008), the influence of these two, possibly ongoing, effects depends upon the viscosity of the mantle that is yet poorly constrained (Plesa et al., 2018) (see Text S5 and Figure S6).

In our simulations, the maximum allowed central deflection of the lithosphere is about 400 m and less than 200 m outside of the polar cap, giving a maximum cap thickness of about 3,500 m. For our range of acceptable solutions, the deflected volume ranges from 0.19 to $0.41 \times 10^6 \text{ km}^3$, and the total north polar cap volume is 1.51 to $1.73 \times 10^6 \text{ km}^3$, which is 15% to 30% higher than previous estimates (Selvans et al., 2010).

The inferred compositions suggest that there must be at least 10 vol% of solid CO_2 (0.15 to $0.17 \times 10^6 \text{ km}^3$, 59 to 67 mbar) within the polar cap if the dust content is larger than 6 vol%, as suggested by the radar estimates of Nerozzi and Holt (2019), the rest being water ice. Increasing the dielectric constant of water ice (from 3 to 3.15, e.g., Grima et al., 2009) or that of the dust (from 6 to 8.8, e.g., Nerozzi & Holt, 2019), or adding more dust to the polar cap, would require an even larger solid CO_2 content. Because of the strong feedback between the polar caps and the atmosphere, having an important amount of sequestered CO_2 , 10 times larger than what was detected at the south pole (Phillips et al., 2011), has important implications on the reconstruction and prediction of the climate evolution of the planet (Levrard et al., 2007).

Acknowledgments

We thank Isaac B. Smith for helpful discussions and Andrew J. Dombard and an anonymous reviewer for their thoughtful comments. The radar data and the polar cap thickness as predicted by MOLA in this paper are available online (<https://doi.org/10.5281/zenodo.3530693>). The radar and topography data used in this paper are available on the PDS Geoscience node (<http://pds-geosciences.wustl.edu/>). A. B. conceived the study with M. W., A. B. and W. F. analyzed the radar data, and all authors contributed to drafting the manuscript. W. F. is supported by the B-type Strategic Priority Program of the Chinese Academy of Sciences (XDB41000000) and Beijing Municipal Science and Technology Commission (Z191100004319001), and the contribution of M. W. is supported by the French Space Agency (CNES). This is InSight contribution number 149. The ternary plots were made using the python-ternary package of Harper et al. (2015).

References

- Belleguic, V., Lognonné, P., & Wieczorek, M. A. (2005). Constraints on the Martian lithosphere from gravity and topography data. *Journal of Geophysical Research*, *110*, E11005. <https://doi.org/10.1029/2005JE002437>
- Broquet, A., & Wieczorek, M. A. (2019). The gravitational signature of Martian volcanoes. *Journal of Geophysical Research: Planets*, *124*, 2054–2086. <https://doi.org/10.1029/2019JE005959>
- Byrne, S. (2009). The polar deposits of Mars. *Annual Review of Earth and Planetary Sciences*, *37*(1), 535–560. <https://doi.org/10.1146/annurev.earth.031208.100101>
- Fegyveresi, J. M., Alley, R. B., Fitzpatrick, J. J., Cuffey, K. M., McConnell, J. R., Voigt, D. E., et al. (2016). Five millennia of surface temperatures and ice core bubble characteristics from the WAIS Divide deep core, West Antarctica. *Paleoceanography*, *31*, 416–433. <https://doi.org/10.1002/2015PA002851>
- Grima, C., Kofman, W., Mouginit, J., Phillips, R. J., Hérique, A., Biccari, D., et al. (2009). North polar deposits of Mars: Extreme purity of the water ice. *Geophysical Research Letters*, *36*, L03203. <https://doi.org/10.1029/2008GL036326>
- Hahn, B. C., McLennan, S. M., & Klein, E. C. (2011). Martian surface heat production and crustal heat flow from Mars Odyssey Gamma-Ray spectrometry. *Geophysical Research Letters*, *38*, L14203. <https://doi.org/10.1029/2011GL047435>
- Harper, M., Weinstein, B., Simon, C., Chebee7i, S. H., Swanson-Hysell, N., Gitter, B., et al. (2015). python-ternary: Ternary plots in Python. *Zenodo*, *12*, 17. <https://doi.org/10.5281/zenodo.34938>
- Herkenhoff, K. E., Byrne, S., Russell, P. S., Fishbaugh, K. E., & McEwen, A. S. (2007). Meter-scale morphology of the north polar region of Mars. *Science*, *317*(5845), 1711–1715. <https://doi.org/10.1126/science.1143544>
- Herkenhoff, K. E., & Plaut, J. J. (2000). Surface ages and resurfacing rates of the polar layered deposits on Mars. *Icarus*, *144*(2), 243–253. <https://doi.org/10.1006/icar.1999.6287>
- Holt, J., Fishbaugh, K. E., Byrne, S., Christian, S., Tanaka, K., Russell, P. S., et al. (2010). The construction of Chasma Boreale on Mars. *Nature*, *465*, 446–449. <https://doi.org/10.1038/nature09050>
- Levrard, B., Forget, F., Montmessin, F., & Laskar, J. (2007). Recent formation and evolution of northern Martian polar layered deposits as inferred from a Global Climate Model. *Journal of Geophysical Research*, *112*, E06012. <https://doi.org/10.1029/2006JE002772>
- McNutt, M. K. (1984). Lithospheric flexure and thermal anomalies. *Journal of Geophysical Research*, *89*(B13), 180–194. <https://doi.org/10.1029/JB089iB13p11180>

- Mellon, M. T. (1996). Limits on the CO₂ content of the Martian polar deposits. *Icarus*, *124*(1), 268–279. <https://doi.org/10.1006/icar.1996.0203>
- Nerozzi, S., & Holt, J. W. (2019). Buried ice and sand caps at the north pole of Mars: Revealing a record of climate change in the cavi unit with SHARAD. *Geophysical Research Letters*, *46*, 7278–7286. <https://doi.org/10.1029/2019GL082114>
- Nunes, D. C., & Phillips, R. J. (2006). Radar subsurface mapping of the polar layered deposits on Mars. *Journal of Geophysical Research*, *111*, E06S21. <https://doi.org/10.1029/2005JE002609>
- Ojha, L., Karimi, S., Lewis, K. W., Smrekar, S. E., & Siegler, M. (2019). Depletion of heat producing elements in the Martian mantle. *Geophysical Research Letters*, *46*, 12,756–12,763. <https://doi.org/10.1029/2019GL085234>
- Ojha, L., Nerozzi, S., & Lewis, K. (2019). Compositional constraints on the north polar cap of Mars from gravity and topography. *Geophysical Research Letters*, *46*, 8671–8679. <https://doi.org/10.1029/2019GL082294>
- Phillips, R. J., Davis, B. J., Tanaka, K. L., Byrne, S., Mellon, M. T., Putzig, N. E., et al. (2011). Massive CO₂ ice deposits sequestered in the south polar layered deposits of Mars. *Science*, *332*(6031), 838–841. <https://doi.org/10.1126/science.1203091>
- Phillips, R. J., Zuber, M. T., Smrekar, S. E., Mellon, M. T., Head, J. W., Tanaka, K. L., et al. (2008). Mars north polar deposits: Stratigraphy, age, and geodynamical response. *Science*, *320*(5880), 1182–1185. <https://doi.org/10.1126/science.1157546>
- Picardi, G., Plaut, J. J., Biccari, D., Bombaci, O., Calabrese, D., Cartacci, M., et al. (2005). Radar soundings of the subsurface of Mars. *Science*, *310*(5756), 1925–1928. <https://doi.org/10.1126/science.1122165>
- Plesa, A.-C., Padovan, S., Tosi, N., Breuer, D., Grott, M., Wieczorek, M. A., et al. (2018). The thermal state and interior structure of Mars. *Geophysical Research Letters*, *45*, 12,198–12,209. <https://doi.org/10.1029/2018GL080728>
- Putzig, N. E., Phillips, R. J., Campbell, B. A., Holt, J. W., Plaut, J. J., Carter, L. M., et al. (2009). Subsurface structure of Planum Boreum from Mars Reconnaissance Orbiter Shallow Radar soundings. *Icarus*, *204*(2), 443–457. <https://doi.org/10.1016/j.icarus.2009.07.034>
- Selvans, M. M., Plaut, J. J., Aharonson, O., & Safaenili, A. (2010). Internal structure of Planum Boreum, from Mars advanced radar for subsurface and ionospheric sounding data. *Journal of Geophysical Research*, *115*, E09003. <https://doi.org/10.1029/2009JE003537>
- Sihvola, A. (2000). Mixing rules with complex dielectric coefficients. *Subsurface Sensing Technologies and Applications*, *1*(4), 393–415. <https://doi.org/10.1023/A:1026511515005>
- Smith, & Wessel (1990). Gridding with continuous curvature splines in tension. *Geophysics*, *55*(3), 293–305. <https://doi.org/10.1190/1.1442837>
- Smith, Zuber, M. T., Frey, H. V., Garvin, J. B., Head, J. W., Muhleman, D. O., et al. (2001). Mars Orbiter Laser Altimeter: Experiment summary after the first year of global mapping of Mars. *Journal of Geophysical Research*, *106*(E10), 23,689–23,722. <https://doi.org/10.1029/2000JE001364>
- Smrekar, S. E., Lognonné, P., Spohn, T., Banerdt, W. Bruce, Breuer, D., Christensen, U., et al. (2018). Pre-mission InSights on the interior of Mars. *Space Science Reviews*, *215*(1), 3. <https://doi.org/10.1007/s11214-018-0563-9>
- Thiriet, M., Michaut, C., Breuer, D., & Plesa, A.-C. (2018). Hemispheric dichotomy in lithosphere thickness on Mars caused by differences in crustal structure and composition. *Journal of Geophysical Research: Planets*, *123*, 823–848. <https://doi.org/10.1002/2017JE005431>
- Wieczorek, M. A. (2008). Constraints on the composition of the Martian south polar cap from gravity and topography. *Icarus*, *196*, 506–517. <https://doi.org/10.1016/j.icarus.2007.10.026>
- Zuber, M. T., Phillips, R. J., Andrews-Hanna, J. C., Asmar, S. W., Konopliv, A. S., Lemoine, F. G., et al. (2007). Density of Mars' south polar layered deposits. *Science*, *317*(5845), 1718–1719. <https://doi.org/10.1126/science.1146995>